NANO LETTERS

2004
Vol. 4, No. 5
957−961

Gap-Dependent Optical Coupling of Single "Bowtie" Nanoantennas Resonant in the Visible

David P. Fromm,[†] Arvind Sundaramurthy,[‡] P. James Schuck,[†] Gordon Kino,[‡] and W. E. Moerner*,[†]

Department of Chemistry, and Department of Electrical Engineering, Stanford University, Stanford, California 94305

Received January 8, 2004; Revised Manuscript Received March 8, 2004

ABSTRACT

Metallic "bowtie" nanoantennas consisting of two opposing tip-to-tip Au triangles have been fabricated with triangle lengths of 75 nm and gaps ranging from 16 to 488 nm. For light polarized along the line between the two triangles, the plasmon scattering resonance first blue-shifts with increasing gap, and then red-shifts as the particles become more and more uncoupled, while perpendicularly polarized excitation shows little dependence upon gap size. This behavior may be approximately understood in a coupled-dipole approximation as changes in the phase between static dipole−dipole interactions and dipole radiative interaction effects.

Researchers have long investigated methods to overcome the diffraction limit, which bounds the lateral resolution of an optical system to $\sim \lambda/(2\ \mathrm{NA})$ with λ the optical wavelength and NA the numerical aperture. Aperture-based near-field techniques, where light is squeezed through a tiny hole, can achieve lateral spatial resolution on the order of the hole diameter.[1] In practice, near-field microscopic images have been recorded by modified optical fiber tips, but these are fragile and plagued by poor transmission, on the order of 10^{-6} for pulled metal-coated fiber probes.[2] Antenna theory predicts that electric fields (E-fields) are enhanced in close proximity to sharpened metal points with a radius of curvature much smaller than the incident illumination wavelength, the so-called lightning-rod effect that has been recently applied at optical frequencies, producing lateral resolution on the order of the curvature of the point.[3] The E-field enhancement in apertureless near-field systems has been exploited to produce an ultra-small, ultra-intense light source that has applications in high-density optical storage, high-resolution optical imaging, and laser spectroscopy, including enhanced fluorescence[4] and Raman scattering.[5]

Small metallic particles with sharp points also produce locally enhanced E-fields, and rod-shaped and triangular antennas have recently been made resonant in the infrared.[6] In the microwave regime, it has been shown that a "bowtie" shaped antenna, where two metallic triangles facing tip-to-tip are separated by a small gap, produces a large E-field confined to the area near the gap.[7] Small gaps between two nanometer-scale particles have also been implicated in producing electromagnetically enhanced "hot spots," enabling the detection of surface enhanced Raman scattering (SERS) of single molecules.[8] However, all single-molecule SERS studies to date have used randomly deposited colloidal particles, and SERS would greatly benefit from metallic nanoparticles of controllable shape and size designed to produce strongly enhanced E-fields.[9] This has motivated a renewed interest in particle scattering studies, with the aim of understanding the near-field coupling of closely spaced metallic particles much smaller than the optical wavelength.

Recently, it has been shown that touching pairs of Ag nanoparticles have a strongly red-shifted scattering spectrum when light is polarized along the pair, i.e., parallel to the axis that joins the nanoparticle centers, but the spectrum resembles single-particle scattering when the polarization is perpendicular to the particle pair.[10] Coupling effects have also been explored as a function of gap length in lithographically produced samples for both arrays of particles[11,12] and even for single pairs of particles.[13] In this paper, we describe the lithographic production of coupled-particle "bowtie" antennas, resonant at optical frequencies, and investigate the resonant scattering spectra of single bowties with gaps varying over a large range to better understand the electromagnetic and plasmon properties of these antennas. This is the first report to our knowledge of both the coupling-dependent blue-shift as well as the red-shift of the peak scattering wavelength for individual metallic bowtie antennas.

* Corresponding author. E-mail: wmoerner@stanford.edu
[†] Department of Chemistry.
[‡] Department of Electrical Engineering.

10.1021/nl049951r CCC: $27.50 © 2004 American Chemical Society
Published on Web 03/25/2004

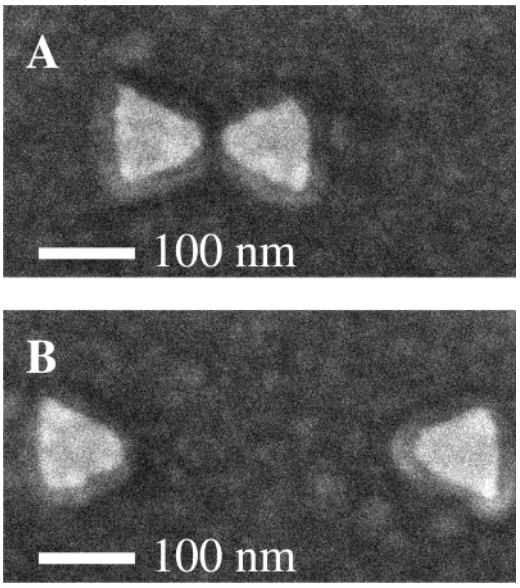

Figure 1. SEM images of representative bowtie antennas. Each bowtie is composed of two opposing, 75 nm-long triangles, with gaps of 20 nm (A) and 285 nm (B). The Au films are 20 nm thick with a 5 nm Cr adhesion layer and are deposited onto an ITO-coated fused silica coverslip. The "halo" of lighter contrast around the particles is likely due to charging induced during SEM imaging and is ignored when determining dimensions.

Au bowties were fabricated with electron beam lithography (EBL) on a transparent substrate using a commercial EBL tool (Raith 150), located at the Stanford Nanofabrication Facility. Substrates consisted of a 160 μm thick fused silica coverslip ($n = 1.47$), overcoated with 50 nm of indium tin oxide (ITO) to reduce charging effects during EBL. Goodberlet et al.[14] demonstrated the ability to write line widths of 19 nm with this tool using single pass lines. The bowties were laid out using single pass lines to reduce proximity effects, thus increasing EBL resolution. Prior to EBL writing, the sample was cleaned in acetone and baked in an oven at 150° C for 2 h to remove moisture. A 50 nm-thick layer of poly-methyl-methacrylate (PMMA) (1% in chlorobenzene, 950,000 m.w.) was spun on the ITO layer and the sample was baked in an oven at 150° C for 2 h to harden the resist and remove residual solvent. During EBL, the resist was patterned at an acceleration voltage of 10 kV and a dose of 275 pC/cm. After exposure, the resist was developed at 22° C using a 25% methyl-iso-butyl-ketone in isopropyl alcohol solution for 28 s. Following development, the sample was plasma-etched in O_2 (100 sccm, 200 mT, 85 V) for 5 s to remove residual resist. A 5 nm Cr adhesion layer and 20 nm Au layer were then deposited using an electron-beam evaporator, with the metal film thickness measured by a quartz crystal monitor, and the patterns were transferred to the substrate via a lift-off process with acetone.

Scanning electron microscope (SEM) images of representative bowties acquired with 2 nm lateral resolution are shown in Figure 1. For this study, the dimensions of each constituent triangle of a bowtie were held constant at 75 $\pm$ 5 nm in length (the distance from the midpoint of the triangle base to its apex), gap lengths were varied from 16 nm to nearly 500 nm, and the triangular tips were observed to have a radius of curvature of 18 $\pm$ 2 nm with a half-angle of 32 $\pm$ 3 degrees. The "halo" around the nanostructures shown in Figure 1 is due to charging effects that occur while obtaining slow-scan, high-resolution SEM images. Single bowties were separated by 10 μm in both directions to eliminate long-range coupling effects and to ensure that scattering from a single bowtie was collected.

Single bowtie scattering spectra are measured with far-field total internal reflection (TIR) microscopy with an inverted microscope. Light from a 30 W tungsten halogen lamp is passed through a 455 nm long-pass filter and coupled into a multimode fiber (65 μm core), which serves as a spatial filter. The fiber output is collimated and focused into a fused silica prism. Index matching fluid ($n = 1.47$) couples the prism to the bottom of the fused silica substrate, placing the Au bowties at the ITO−air interface. For all experiments, the excitation light is s-polarized and the axis of each bowtie is carefully oriented either parallel or perpendicular to the polarization axis. When the bowties are not present, the excitation is confined to the evanescent field and no light is detected in the far-field with the microscope. When a bowtie is present in the evanescent field, far-field scattered light is collected with an air objective (100×, 0.8 NA), and a 50 μm pinhole is placed at the microscope image plane to spatially filter the collected light to an area ~0.5 μm diameter on the sample plane. The particles are located by scanning the sample stage and observing the broadband scattered light collected with a single-photon counting avalanche Si photodiode. Spectra are acquired by dispersing the scattered light with a 150 lines/mm grating monochromator onto a liquid nitrogen-cooled charged coupled device Si detector in a single 60 s camera exposure. All spectra presented in this study are corrected for the wavelength and polarization dependences of the lamp emission, optical system throughput, and detector quantum efficiency.

Optical excitation of the bowties excites the plasmon resonance of the structure, which may be sensed in the wavelength dependence of the scattering spectra. Figure 2 shows the scattering spectra of five different bowtie antennas, covering a spectral range from 480 to 910 nm, with the polarization oriented along (A) and orthogonal to (B) the axis of the bowtie. The spectra have varying line shapes and peak amplitudes, revealing heterogeneity among individual bowties fabricated at high resolution (see below), so the primary variable we interpret is the peak wavelength. Strong gap-dependent spectral shifts are evident for bowties pumped along their long axes. For gap sizes less than 100 nm, the spectra blue-shift as gap size increases, from a peak wavelength of 830 nm (17 nm gap) to 720 nm (97 nm gap). However, at gaps larger than 100 nm, the spectra red-shift with increasing gap lengths; a bowtie with a 485 nm gap produces a resonance at 795 nm. For spectra acquired when the excitation light is polarized perpendicular to the bowtie's long axis, the peak scattering wavelength varies little with increasing gap lengths, though the scattering intensity decreases with increasing gap size. After scattering spectra were measured for a given bowtie at both polarizations, the shape and length of a given structure were characterized with

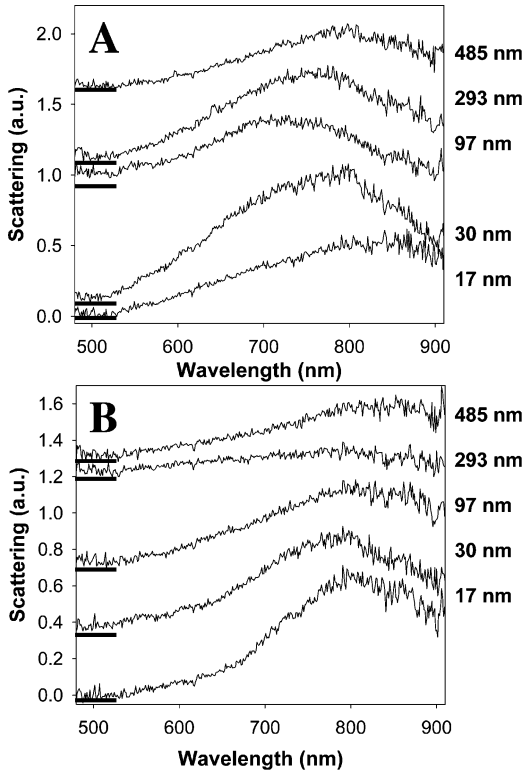

Figure 2. Scattering spectra for five individual metallic bowtie antennas, with the incident illumination polarized parallel (A) and perpendicular (B) to the long axis of the bowtie. Gap sizes are indicated at the right of each spectrum, and all spectra are normalized to the same maximum intensity (relative intensities have not been changed), but are offset for clarity. The zero level is indicated for each spectrum.

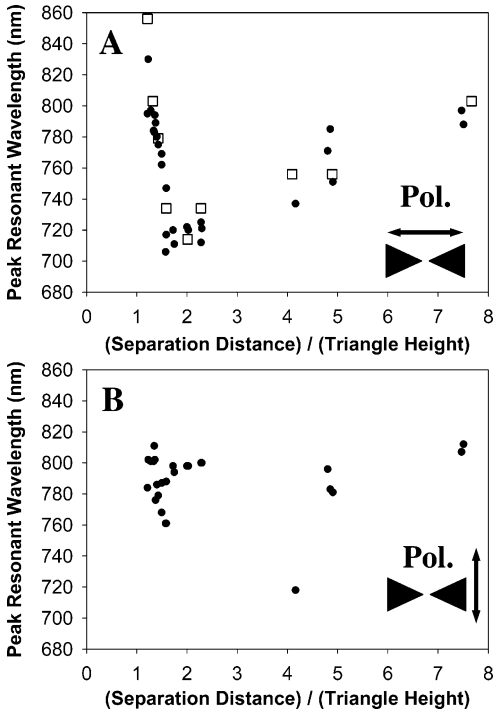

Figure 3. Experimental measurements (closed circles) and FDTD simulations (open squares) of the peak scattering wavelength versus the ratio, r, of center−center distance to triangle length for incident illumination parallel (A) and perpendicular (B) to the antenna axis. The peak experimental wavelengths are determined with ± 10 nm uncertainty. Note the minimum in panel (A) at $r \sim 2$. FDTD simulations are presented for incident light polarized parallel to the antenna axis only and are in excellent agreement with the experimental observations.

an SEM. It should be noted that performing SEM imaging on a bowtie before measuring its scattering spectrum significantly alters the scattering properties of the particles, indicating that SEM imaging changes the composition of the Au particles. Therefore, all SEM imaging was done after measuring scattering spectra.

Plotting the peak resonant wavelength as a function of the separation distance provides further insight into the interparticle coupling behavior of single bowtie antennas. Figure 3 shows the resonant scattering wavelength for 27 individual bowties fabricated in the same production run, with gaps ranging from 16 to 488 nm, plotted against r, the dimensionless ratio of center−center distance (taken as 75 nm plus the gap length) divided by triangle length (particles that are touching would have $r = 1$). The scattering resonances of bowties pumped along their long axes (Figure 3A) show a strong dependence on the gap length, indicating considerable coupling between the plasmon resonances of the two triangles. At the shortest gaps, $r = 1.23$ (17 nm gap), the plasmon resonance is 830 ± 10 nm, and the spectra sharply blue-shift as the gap increases until $r = 1.6$ (45 nm gap, 705 ± 10 nm plasmon resonance). For still larger gaps, the spectra red-shift with increasing separation distance, until the particles begin to decouple for $r = 7.50$ (488 nm gap), where the spectrum is peaked at 790 ± 10 nm. Bowties pumped orthogonal to their long axis (Figure 3B) show considerably different gap dependence. Most bowties have plasmon resonances near the uncoupled value of 790 nm, though there may be a modest red-shift as r increases. It should be noted that bowties fabricated in different runs displayed a similar trend in their gap-dependent scattering response, though other samples were restricted to a smaller gap range. The scatter in both panels of Figure 3 exceeds the uncertainty in the peak wavelength measurement and is likely due to the heterogeneity that exists among single antennas, which is dependent on several factors, including particle shape and orientation, local film thickness, local substrate effects, and the lattice structure of the Au. Particles that appear the same with SEM imaging can behave quite differently, demonstrating the sensitivity of the bowtie coupling effects to the precise shape, roughness, and local environment of the metallic structures. Further, the scatter in Figure 3 may also provide some insight to the key factors controlling the nanometer-scale interaction of metallic nanoparticles. The gap-dependent scattering response is more consistent for the smallest gaps when the incident light is polarized along the particle axis (Figure 3A, $1 \leq r \sim 2$) but is less predictable for larger gaps and also when the light is polarized perpendicular to the particle axis. It is conceivable that the coupling is dominated by the capacity of the gap itself at small distances, but the shape and nanoparticle composition become more important at larger separation distances. Thus, nanoscale variations in the particles and the substrate, which are undetectable with the SEM, may have

a greater effect on the scattering response for particles that are more weakly coupled to each other.

Finite difference time domain (FDTD) simulations are also presented in Figure 3A for comparison to the experimental observation. Extensive FDTD simulations have been performed and will be presented in detail elsewhere,[16] but are briefly presented here to demonstrate the strength of this technique to predict the plasmon resonance of coupled nanoparticle systems. Briefly, FDTD software[17] evaluates the electric field distribution in the vicinity of a single bowtie, and this is converted to a far-field extinction efficiency. The simulation is repeated at several wavelengths to determine the resonant wavelength for a given antenna structure. The bowtie structures simulated are of the same gap length, radius of curvature of the tip, film thickness, size, and shape as the bowties measured experimentally, i.e., the particles are modeled to be 20 nm thick Au on 4 nm Cr at the interface of air and 52 nm ITO ($n = 1.95$). Illumination is provided by a plane wave that passes through fused silica ($n = 1.47$) and into the ITO, and the polarization of the incident fields are chosen to mimic the experimental conditions. The simulation data are in remarkable agreement with the experimental observation, as seen in Figure 3A, with plasmon resonances spanning the appropriate wavelength range and the characteristic minimum near $r \sim 2$.

While numerical methods, such as FDTD simulations, can provide accurate predictions of certain properties of nanoparticle systems, other theoretical methods are also important in understanding the physical properties of nanoscale antennas. However, relatively little theoretical modeling has been generated for the electromagnetic coupling of triangular-shaped nanoparticles. Recent experimental and theoretical studies on interparticle-spacing-dependent scattering for other nanoparticle shapes and configurations may provide valuable physical insight into the bowtie antennas which will assist in developing metallic nanostructures with maximally enhanced near fields. Rechberger et al.[12] reported that the spectra of coupled disk-shaped particles pumped along their long axis blue-shift with increasing gap lengths, but this effect subsides for $r > 2$, where the plasmon resonance wavelength remains fairly constant up to $r = 3$, the maximum value studied. The spectra show a slight red-shift when the polarization is perpendicular to the particle axis. The authors explain both effects with a simple dipole−dipole interaction picture. When the particles are excited, they become polarized. When the incident light is polarized along the dimer axis, the charge separation creates an attractive force, lowering the plasmon energy. As the gap length increases, this effect diminishes and the plasmon energy approaches that of a single, isolated particle. For particles pumped orthogonal to the long axis, the polarizability of the particles creates repulsive forces, which are strongest for the smallest gaps, thus explaining the observed red-shift. Su et al.[13] observed blue-shifting spectra with increasing gap lengths, from $r = 1$ to $r = 2.5$, for single, elliptical particles pumped with light polarized along the dimer axis, and explained their results with a tunneling model, whose coupling efficiency falls off exponentially as a function of distance and is predicted to be insignificant for particles with $r > 3.5$.

Other recent work has focused on the gap-dependent plasmon resonances for arrays of disk-shaped and triangular particles arranged in square and hexagonal lattices with periodicities ranging from 200 nm (the particle size) to 500 nm.[11] The authors utilized electrodynamics simulations in the coupled dipole approximation (CDA). Zhao et al.[15] detail a semianalytical method based on CDA theory to understand particle coupling effects in terms of a dimensionless lattice sum, S, given by

$$S = d^3 \sum_{j \neq i} \left[\frac{(1 - ikd_{ij})(3\cos^2\theta_{ij} - 1)e^{ikd_{ij}}}{d_{ij}^3} + \frac{k^2 \sin^2\theta_{ij} e^{ikd_{ij}}}{d_{ij}} \right] \quad (1)$$

where d_{ij} is the distance between particles i and j, θ_{ij} describes the angle between the polarization vector and the vector from particle i to j, d is the lattice spacing, and $k = 2\pi/\lambda$. It was shown that the real part of S describes the plasmon resonance shift, with positive values indicating a red-shift and negative values a blue-shift, and the imaginary part of S describes the width of the resonance, with positive values indicating a broadened line shape compared to an uncoupled particle spectrum. The $1/d^3$ term describes short-range interactions, while the $1/d$ term, describing the radiative dipole interaction, dominates at larger lattice spacing. Most notably, each term oscillates in phase as the retardation factor, e^{ikd}. Because of this oscillating retardation, the authors predict a blue-shift in the scattering spectra for two-dimensional arrays with small d, where the large, positive $1/d^3$ term dominates S, but a red-shift for larger d, when e^{ikd} changes sign and the $1/d$ term becomes dominant. The CDA approach appears to be qualitatively robust, agreeing well with other theoretical methods;[15] however, only the red-shifting behavior is seen experimentally in array samples.

To lowest order, it is conceivable to consider a bowtie antenna as a one-dimensional system of two dipoles. For a one-dimensional dipole system, the $1/d$ term vanishes when the light is polarized parallel to the long axis, since $\sin\theta_{ij} = 0$, which would indicate only a short-range, $1/d$,[3] dependence on the plasmon resonance. Indeed, the one-dimensional dipole−dipole interaction model appears to explain the gap-dependent blue-shifting spectral trends seen over the range of gaps studied thus far for disc-shaped[12] and elliptical particles,[13] but it fails to explain the red-shifting behavior that we observe for the bowties with large (> 100 nm) gaps pumped along their axes.

Alternatively, one can treat each triangular constituent of the bowtie as a finite, two-dimensional array of small dipoles and use existing theory for infinite two-dimensional arrays to extrapolate to our system, and with this approximation, the CDA qualitatively agrees with the gap-dependent spectra that we observe. Most notably, for bowties pumped with incident light polarized along their axes, there is clear evidence of an oscillating retardation effect, as evidenced by the minimum seen in Figure 3A for $r \sim 2$. According to refs 11 and 15, the wavelength at which the blue-shift

becomes a red-shift for an array of particles behaving as dipoles is largely determined by the criterion $2\pi D/\lambda_{plasmon} \approx 1$. Hence, D defines the nearest neighbor distance where the $1/d$ term begins to determine the plasmon resonance and $\lambda_{plasmon}$ is the uncoupled particle plasmon wavelength. While the CDA theory was developed for a different system, evaluating this expression for our system, using $\lambda_{plasmon} =$ 800 nm, yields a center-to-center spacing, $D = 127$ nm, corresponding to $r = 1.7$, in surprisingly good agreement with our observed results considering the various approximations made in the CDA theory. Additionally, the slope of the plot is much larger for small gaps than for large gaps, which is reasonable considering the $1/d^3$ term in S. Thus, it appears that each constituent triangle of a bowtie antenna can be thought of as a collection of small coupled dipoles, arranged in a finite two-dimensional lattice, though further CDA and FDTD[17] simulations should provide more insight into this possibility. We would anticipate that coupled particles of other shapes, including the disc-shaped and elliptical particles previously studied,[12,13] would behave similar to bowtie antennas, provided a larger range of gap lengths were available for observation, though triangular particles may display stronger coupling effects due to their relatively sharp points, which should foster higher local charge densities due to the lightning rod effect.

In summary, we have produced isolated Au bowtie antennas with 75 nm triangle lengths on transparent substrates using electron-beam lithography. We have observed resonant scattering spectra from single bowties using total internal reflection microscopy, observing a strong polarization and gap-dependent scattering response. Bowties excited with polarization along their long axes have plasmon resonances that strongly blue-shift with increasing gap size, until the center-to-center particle spacing is ~2 times the length of an individual triangle, at which time the spectra red-shift with increasing gap size. This coupling effect remains noticeable even when particles are spaced by 7 times the particle length, and FDTD simulations agree quite well with experimental observations, suggesting their utility in predicting the behavior of other coupled nanoparticle systems. Bowties pumped perpendicular to their long axes show a gradual decrease in their total scattering intensity and may exhibit a modest red-shift in their plasmon resonance with increasing gap spacing. The coupling effects seen for bowties can be qualitatively explained by a two-dimensional coupled dipole approximation that was first developed to predict the scattering spectra for nanoparticle arrays. The resonances of such bowtie structures should be accompanied by enhanced local fields that may be useful in future nanoscale imaging applications.

Acknowledgment. D.F. thanks the NSF for a Graduate Research Fellowship, and A.S. thanks Ken Crozier for assistance with sample preparation. This work was supported by the National Institutes of Health Grant No. GM65331-R21 and the Department of Energy Grant No. DE-FG03-00ER45815. The authors also thank Prof. George Schatz for valuable discussions.

References

(1) Synge, E. H. *London, Edinburgh Dublin Philos. Mag. J. Sci.* **1928**, *6*, 356.
(2) Betzig, E.; Trautman, J. K.; Harris, T. D.; Weiner, J. S.; Kostelak, R. L. *Science* **1991**, *251*, 146.
(3) Novotony, L.; Bian, R. X.; Xie, X. S. *Phys. Rev. Lett.* **1997**, *79*, 645.
(4) Hamann, H. F.; Kuno, M.; Gallagher, A.; Nesbitt, D. J. *J. Chem. Phys*. **2001**, *114*, 8596.
(5) Hartschuh, A.; Sanchez, E. J.; Xie, X. S.; Novotny, L. *Phys. Rev. Lett*. **2003**, *90*, 095503−1.
(6) Crozier, K. B.; Sundaramurthy, A.; Kino, G. S.; Quate, C. F. *J. Appl. Phys*. **2003**, *94*, 4632.
(7) Grober, R. D.; Schoelkopf, R. J.; Prober, D. E. *Appl. Phys. Lett*. **1997**, *70*, 1354.
(8) Michaels, A. M.; Jiang, J.; Brus, L. *J. Phys. Chem. B* **2000**, *104*, 11965.
(9) Li, K.; Stockman, M. I.; Bergman, D. J. *Phys. Rev. Lett.* **2003**, *91*, 227402.
(10) Tamaru, H.; Kuwata, H.; Miyazaki, H. T.; Miyano, K. *Appl. Phys. Lett*. **2002**, *80*, 1826.
(11) Haynes, C. L.; McFarland, A. D.; Zhao, L.; Van Duyne, R. P.; Schatz, G. C.; Gunnarson, L.; Prikulis, J.; Kasemo, B.; and Kall, M. *J. Phys. Chem. B* **2003**, *107*, 7337.
(12) Rechberger, W.; Hohenau, A.; Leitner, A.; Krenn, J. R.; Lamprecht, B.; Ausenegg, F. R. *Opt. Commun.* **2003**, *220*, 137.
(13) Su, K. H.; Wei, Q.-H.; Zhang, X.; Mock, J. J.; Smith, D. R.; Schultz, S. *Nano Lett.* **2003**, *3*, 1087.
(14) Goodberlet, J. G.; Hastings, J. T.; Smith, H. I. *J. Vac. Sci. Technol. B* **2001**, *19*, 2499.
(15) Zhao, L.; Kelly, K. L.; Schatz, G. C. *J. Phys. Chem. B* **2003**, *107*, 7343.
(16) Sundaramurthy, A.; Fromm, D. P.; Crozier, K. B.; Schuck, P. J.; Moerner, W. E.; Kino, G. S., manuscript in preparation.
(17) The FDTD package used is TEMPEST 6.0, Electronics Research Laboratory, University of California at Berkeley.

NL049951R